

Cumulus Convection in the Atmosphere with Vertical Wind Shear : Numerical Experiment

By Tomio Asai

Meteorological Research Institute
(Manuscript received 15 June 1964)

Abstract

The behavior of cumulus convection in a prevailing wind with vertical shear is studied by integrating a set of dynamic equations numerically. The motion is considered under the solenoidal condition in a vertical two dimensional plane. Aside from the eddy exchange, the pseudo-adiabatic process is assumed in which the motion is moist adiabatic in saturated ascending air and dry adiabatic in the remaining air.

The comparison between both cases, with and without vertical shear, is made concerning the time dependent evolution of convections and their energy conversion. In a prevailing wind field with vertical shear, the axial symmetry of the convection is destroyed and the axis of the convection cell tilts downwind with height. This results in the interaction between the convective motion and the prevailing wind which transforms the kinetic energy of the convection into that of the prevailing wind. Therefore, vertical wind shear tends to suppress the development of the convection in the vertical plane parallel to the wind. Moreover, the discrepancy which develops between the central axes of updraft and the warm regions of the convection decreases the conversion of potential to kinetic energy—one which contributes to the development of the convection.

1. Introduction

Recently, some numerical experiments of cumulus convection have been made by some authors (Malkus and Witt, 1959 ; Ogura, 1962, 1963 ; Lilly, 1962 ; Chao, 1961 ; Asai, 1960, 1964, etc.) to study dynamically the time dependent evolution of cumulus. All of these experiments, however, were concerned with axial or slab symmetric convection in a stratified fluid layer, initially at rest*. From a meteorological point of view, there should be considerable interest in cumulus convection in a prevailing wind, especially with vertical shear.

Jeffreys (1928) suggested that a basic current with vertical shear stabilizes all modes of the perturbations parallel to the current except for one mode of infinite wave length

* According to Dr. Koo, Institute of Geophysics and Meteorology, Academia Sinica, who visited Japan last December, a numerical experiment has been made for convection in a prevailing wind with vertical shear by Chao and Chen.

in unstably stratified fluid layer. Therefore, he stated that the convective disturbance occurs in strips instead of in the symmetrical Benard cells which are observed in laboratory experiments (for example, see Brunt (1951)). Kuettner (1959) illustrated many observational examples of cloud streets oriented in the direction of the prevailing wind in the atmosphere. These were attributed to a dynamical prohibiting effect of curvature of wind profile with height on the convection. Conover (1960) also supported Kuettner's theory based upon photographic observation of cirrus patterns near the jet stream. Byers and Braham (1949) regarded wind shear as a destroying force in the report of the Thunderstorm Project. Newton (1959) indicated, however, the important role of vertical wind shear in intensifying and prolonging the convection, specifically, in a large, organized convective storm. In the recent severe storm conference, Ludlum (1963) stated that wind shear is unfavorable for cumulus development but not for vigorous

cumulonimbus convection. Namely it is implied that the influence of the vertical shear on an isolated convection may not always be the same as that on a large organized convective system. Most recently Chao (1962) and Kuo (1963) showed the suppressive effect of vertical shear on convection by making use of linear theory.

Slanting cumulus downshear with height has been clearly seen in numerous photographs and radar observations, with the updraft area of cumulus development not coincident with cumulus cloud. It is pointed out, however, by some authors (Hitschfeld (1960), Browning and Ludlam (1962)) that a large cumulonimbus is nearly always found to be upright or slanting upshear side with height into the prevailing wind. Then Ludlam provided a model including the air flow sustained by the above observational results, especially detailed analysis of a large hail storm by radar observation.

Finally we must mention the meteorological experience that cumulus moves nearly with the wind velocity at some level which corresponds to the mean wind of the layer including it (Ligda, 1956; Byers and Battan, 1949, etc.), though it is not so simple for an organized large cumulonimbus (Newton, 1959, etc.).

Hence, it seems desirable to make a consistent physical model taking into account the interaction between the convection and the prevailing wind. This, however, will introduce various complexities and difficulties into the solution of the dynamical and cloud physical processes. In this paper our attention will be devoted to the dynamical effect of a prevailing wind with vertical shear on the development, the displacement and configuration of a cumulus convection.

2. A set of governing equations

The basic assumptions adopted here are the same as those in another paper by the present author (1964). First of all the pseudo-adiabatic process is assumed with the exception of the eddy exchange. Thus the moist adiabatic process is followed in the saturated ascending area and dry adiabatic in the other. The motion is assumed to be solenoidal in order to eliminate noise motion with higher

frequency such as an acoustic wave. The effect of the pressure fluctuation induced by the convective motion will be neglected in the equations concerned with the thermodynamics and the saturation specific humidity. Then, the governing system of equations obtained will be expected to be similar to that of so called "shallow convection" derived by Spiegel and Veronis (1960) and Ogura and Phillips (1962). The Fickian type of diffusion of momentum, heat and water vapor is introduced in order to take into account the mixing through much smaller scale eddies than the convection under consideration. All of the coefficients of eddy diffusion are assumed to be the same constant, $10^2 \text{ m}^2 \text{ sec}^{-1}$, in both space and time. Finally, the motion is confined to the vertical two dimension (x, z) in which x and z are the horizontal and the vertical coordinate axes, respectively.

Under these conditions we can obtain the following set of equations:

$$\frac{\partial}{\partial t} \nabla^2 \psi = J(\psi, \nabla^2 \psi) - g \frac{\partial T^*}{\partial x} + \mu \nabla^4 \psi^* \quad (2.1)$$

$$\frac{\partial T^*}{\partial t} = J(\psi, T^*) + S_0 \frac{\partial \psi}{\partial x} + \mu \nabla^2 T^* \quad (2.2)$$

$$\frac{\partial q}{\partial t} = J(\psi, q) + \mu \nabla^2 q^* - \frac{\partial m}{\partial t} \quad (2.3)$$

$$\frac{\partial q_s}{\partial t} = \frac{Lq_s}{R_v T_0} \frac{\partial T^*}{\partial t} \quad (2.4)$$

$$\frac{\partial m}{\partial t} = \begin{cases} 0 & \text{for } q \leq q_s \\ \frac{\partial}{\partial t} (q - q_s) & \text{for } q > q_s \end{cases} \quad (2.5)$$

The first equation (2.1) is the horizontal component perpendicular to the vertical $x-z$ plane of the vorticity equation. The velocity components u and w can be represented in terms of stream function ψ :

$$u = \frac{\partial \psi}{\partial z}, \quad w = -\frac{\partial \psi}{\partial x} \quad (2.6)$$

Here
$$J(A, B) = \frac{\partial A}{\partial x} \frac{\partial B}{\partial z} - \frac{\partial A}{\partial z} \frac{\partial B}{\partial x}$$

and
$$\nabla^2 = \frac{\partial^2}{\partial x^2} + \frac{\partial^2}{\partial z^2}$$

The equation (2.2) is the thermodynamic

equation which can be obtained by neglecting the terms of smaller order of magnitude than T^* defined to be $(T - T_0)/T_0$, that is the percentage deviation of the temperature from its initial horizontal average T_0 . S_0 is the static stability of the initial basic field which is represented by

$$S_0 = \frac{1}{T_0} \left(\left\{ \frac{\Gamma_d}{\Gamma_s} \right\} - \gamma_0 \right) \quad (2.7)$$

where $\Gamma_d = g/C_p$ is the dry adiabatic lapse rate,

$$\Gamma_s = \Gamma_d \left(1 + \frac{L_v q_{s0}}{R_d T_0} \right) / \left\{ 1 + \frac{L_v}{C_p T_0} \left(\frac{L_v}{R_v T_0} - 1 \right) q_{s0} \right\}$$

the moist adiabatic lapse rate and $\gamma_0 = -\partial T_0 / \partial z$ the lapse rate of the initial basic field, respectively. L_v is the latent heat of water vapor, C_p the specific heat of air at constant pressure, R_d the gas constant of dry air and R_v the gas constant of water vapor. Γ_s is adopted in the equation (2.2) only when and where the air ascends in the saturated area as described above.

The equation (2.3) is the continuity equation of moisture, in which q is the specific humidity and m the condensed water content. If the specific humidity q obtained without condensation becomes larger than the saturation specific humidity q_s , determined by the equation (2.4), the excess of water vapor is assumed to condense immediately and to fall out of the system.

It should be noted that ϕ^* and q^* are the deviations from their initial basic fields which

are in a horizontally uniform steady state if there is no convective motion (Asai, 1960). These equations compose a complete set of equations together with the appropriate boundary and the initial conditions described in the following.

3. Boundary conditions

The domain concerned is confined to the rectangular atmospheric layer with the depth of 5 km and the width of 10 km (Fig. 1).

Both upper and lower boundaries are the fixed horizontal planes at which vertical velocity vanishes, *i.e.*,

$$\phi = \text{constant at } z=0 \text{ and } z=H \quad (3.1)$$

Lateral boundary conditions are assumed to be cyclic in all variables,

$$A(L, z) = A(0, z) \quad (3.2)$$

, where $A(x, z)$ is an arbitrary variable. Furthermore the vertical gradients of the variables (u^* , T^* and q^*) are assumed to vanish at the upper and the lower boundaries,

$$\left. \begin{aligned} \frac{\partial u^*}{\partial z} = 0 \\ \frac{\partial T^*}{\partial z} = 0 \\ \frac{\partial q^*}{\partial z} = 0 \end{aligned} \right\} \text{ at } z=0 \text{ and } z=H \quad (3.3)$$

$$\left. \begin{aligned} \frac{\partial T^*}{\partial z} = 0 \\ \frac{\partial q^*}{\partial z} = 0 \end{aligned} \right\} \text{ at } z=0 \text{ and } z=H \quad (3.4)$$

$$\left. \begin{aligned} \frac{\partial q^*}{\partial z} = 0 \end{aligned} \right\} \text{ at } z=0 \text{ and } z=H \quad (3.5)$$

The equations (3.1) and (3.3) result in the relation,

$$\nabla^2 \phi^* = 0 \text{ at } z=0 \text{ and } z=H \quad (3.6)$$

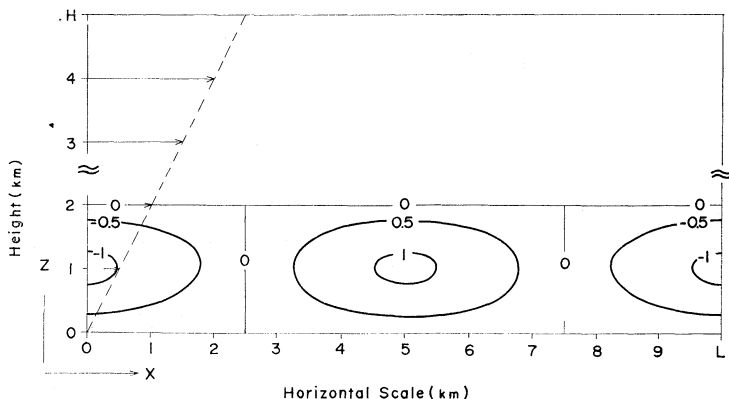


Fig. 1. Domain and initial field adopted in numerical experiment.

Hence, we can eliminate the vertical eddy exchanges of momentum, sensible heat and water vapor through boundaries of the domain and thereby obtain rather simple energy considerations. It was shown, however, by the present author (1964) that some other types of boundary conditions such as rigid ($u^*=0$) and complete conductor (always $T^*=0$ and $q^*=0$) hardly changed the feature of convection.

4. Energy integrals

Multiplying the equation (2.1) by the stream function ϕ and the equation (2.2) by the geopotential ϕ and thus integrating them over the whole domain making use of the boundary conditions mentioned before, we can obtain the kinetic and the potential energy integrals as follows :

$$\frac{\partial}{\partial t} \iint \frac{1}{2} (\nabla \phi)^2 ds = \iint g T^* w ds - \mu \iint \nabla^2 \phi \nabla^2 \phi^* ds \tag{4.1}$$

$$\frac{\partial}{\partial t} \iint (-\phi T^*) ds = - \iint g T^* w ds + \iint \phi s_0 w ds - \mu \iint \phi \nabla^2 T^* ds \tag{4.2}$$

where ds is the area element $dx dz$.

The potential energy should be noted to be defined as the product of ϕ multiplied by the percentage deviation of temperature $-T^*$. The above energy integrals are divided into the mean and the eddy energy integrals in order to illustrate dynamical implication of convection more clearly.

We first introduce the notations of the mean and the eddy fields which are defined, respectively,

$$\bar{A} = \frac{1}{L} \int_0^L A dx \tag{4.3}$$

$$\langle A \rangle = \frac{1}{LH} \int_0^L \int_0^H A dx dz \tag{4.4}$$

as the mean fields of A , and

$$A' = A - \bar{A} \tag{4.5}$$

$$A'' = A - \langle A \rangle \tag{4.6}$$

as the eddy fields of A .

Now we write the equation (2.1) in its horizontally averaged form,

$$\frac{\partial}{\partial t} \frac{\partial^2 \bar{\phi}}{\partial z^2} = J(\overline{\phi'}, \nabla^2 \overline{\phi'}) + \mu \frac{\partial^4 \bar{\phi}^*}{\partial z^4} \tag{4.7}$$

and then subtract this from the equation (2.1) to obtain the deviation form,

$$\frac{\partial}{\partial t} \nabla^2 \phi' = J(\phi, \nabla^2 \phi) - J(\overline{\phi'}, \nabla^2 \overline{\phi'}) - g \frac{\partial T^*}{\partial t} + \mu \nabla^4 \phi' \tag{4.8}$$

When the equation (4.7) is multiplied by $\bar{\phi}$ and is integrated over the domain, we can derive the following equation after some arrangement,

$$\frac{\partial}{\partial t} \iint \frac{1}{2} \left(\frac{\partial \bar{\phi}}{\partial z} \right)^2 ds = - \iint \frac{\partial \phi'}{\partial x} \frac{\partial \phi'}{\partial z} \frac{\partial^2 \bar{\phi}}{\partial z^2} ds - \mu \iint \frac{\partial^2 \bar{\phi}}{\partial z^2} \frac{\partial^2 \bar{\phi}^*}{\partial z^2} ds \tag{4.9}$$

Multiplying the equation (4.8) by ϕ' and integrating over the domain, we can get the following energy integral,

$$\frac{\partial}{\partial t} \iint \frac{1}{2} (\nabla \phi')^2 ds = \iint g T^* w ds + \iint \frac{\partial \phi'}{\partial x} \frac{\partial \phi'}{\partial z} \frac{\partial^2 \bar{\phi}}{\partial z^2} ds - \mu \iint (\nabla^2 \phi')^2 ds \tag{4.10}$$

Following a similar procedure with the equation (2.2), we can derive the mean and the eddy potential energy integrals,

$$\frac{\partial}{\partial t} \iint -\langle \phi \rangle T^* ds = \iint \langle \phi \rangle S_0 w ds \tag{4.11}$$

$$\frac{\partial}{\partial t} \iint -\phi'' T^* ds = - \iint g T^* w ds + \iint \phi'' S_0 w ds - \mu \iint \phi \nabla^2 T^* ds \tag{4.12}$$

Since ϕ depends only upon the vertical coordinate, the mean potential energy defined here is the potential energy averaged over the whole domain which is proportional to internal energy with the opposite sign. The eddy potential energy is the deviation of potential energy from its mean value. Hence,

if warming occurs in the lower layer or cooling in the upper layer, it results in an increase of the eddy potential energy.

For the sake of simplicity the energy integrals described above are summarized in the following abbreviated forms.

$$\frac{\partial}{\partial t} \langle K \rangle = \langle gT^*w \rangle - \langle D_k \rangle \tag{4.13}$$

$$\frac{\partial}{\partial t} \langle K_e \rangle = \langle gT^*w \rangle - \langle uw \frac{\partial \bar{u}}{\partial z} \rangle - \langle D_{ke} \rangle \tag{4.14}$$

$$\frac{\partial}{\partial t} \langle K_m \rangle = \langle uw \frac{\partial \bar{u}}{\partial z} \rangle - \langle D_{km} \rangle \tag{4.15}$$

$$\frac{\partial}{\partial t} \langle P \rangle = - \langle gT^*w \rangle + \langle \phi S_0 w \rangle - \langle D_p \rangle \tag{4.16}$$

$$\frac{\partial}{\partial t} \langle P_e \rangle = - \langle gT^*w \rangle + \langle \phi'' S_0 w \rangle - \langle D_{pe} \rangle \tag{4.17}$$

$$\frac{\partial}{\partial t} \langle P_m \rangle = \langle \phi \rangle \langle S_0 w \rangle \tag{4.18}$$

$$\frac{\partial}{\partial t} \langle K+P \rangle = \langle \phi S_0 w \rangle - \langle D_k \rangle - \langle D_p \rangle \tag{4.19}$$

where

$$\langle K_e \rangle \equiv \frac{1}{2} \langle u'^2 + w'^2 \rangle = \frac{1}{2} \langle (\nabla \phi')^2 \rangle$$

$$\langle K_m \rangle \equiv \frac{1}{2} \langle \bar{u}^2 \rangle = \frac{1}{2} \langle \left(\frac{\partial \bar{\phi}}{\partial z} \right)^2 \rangle$$

$$\langle K \rangle \equiv \langle K_m \rangle + \langle K_e \rangle$$

$$\langle P_e \rangle \equiv - \langle \phi'' T^* \rangle$$

$$\langle P_m \rangle \equiv - \langle \phi \rangle \langle T^* \rangle$$

$$\langle P \rangle \equiv \langle P_m \rangle + \langle P_e \rangle$$

$$\langle D_{ke} \rangle \equiv \langle \mu (\nabla^2 \phi')^2 \rangle$$

$$\langle D_{km} \rangle \equiv \langle \mu \frac{\partial^2 \bar{\phi}}{\partial z^2} \frac{\partial^2 \bar{\phi}^*}{\partial z^2} \rangle$$

$$\langle D_k \rangle \equiv \langle \mu \nabla^2 \phi \cdot \nabla^2 \phi^* \rangle$$

$$\langle D_{pe} \rangle \equiv \langle \mu \phi'' \nabla^2 T^* \rangle$$

$$\langle D_p \rangle \equiv \langle \mu \phi \nabla^2 T^* \rangle = \langle D_{pe} \rangle$$

These expressions make the physical interpretation implied quite clear in a manner similar to that provided by Phillips (1956) in a numerical experiment of general circulation. As known from the equations (4.14) and (4.17), $\langle gT^*w \rangle$ represents a conversion between the eddy potential energy and the eddy kinetic energy. Another important conversion is due to the u, w correlation term $\langle uw (\partial \bar{u} / \partial z) \rangle$ which results from an asymmetric convection in the layer with vertical shear. When the upward transport of horizontal momentum occurs in flow increasing with height, it results in the transformation of the eddy kinetic energy into the mean kinetic energy. Therefore, the evolution of convection will be controlled not only by the temperature field but also by the basic flow.

The effect of the release of latent heat due to condensation is represented by $\langle \phi S_0 w \rangle$ of which negative values correspond to heating and positive value to cooling. If the process is assumed to be either dry or moist adiabatic, for both ascending and descending motion in the entire regions, S_0 becomes constant or depends only upon height and $\langle \phi S_0 w \rangle$ must vanish. In the present case, which is assumed to be pseudo-adiabatic, it does not vanish due to the correlation between S_0 and w . Then all of the released latent heat is available for heating the air. We can notice that the evolution of convection is affected not by the mean heating $-\langle S_0 w \rangle$ but by the vertical distribution of heating $\overline{S_0 w''}$. The reason for this is that the former term affects only the mean potential energy $\langle P_m \rangle$, whereas the latter term can affect the eddy potential energy $\langle P_e \rangle$ and subsequently transformed into the kinetic energy of convection $\langle K_e \rangle$.

Finally $\langle D_k \rangle$ and $\langle D_p \rangle$ represent loss of kinetic energy and of potential energy due to the eddy viscosity and the eddy conduction, respectively. The former is always a loss but the latter is not necessarily a loss in every instance.

5. Computational scheme and initial conditions

A set of differential equations (2.1)–(2.5) are transformed into the finite difference equations in the same way as in the paper

by the present author (1964). The centered difference formulae in both time and space are used except for the forward time difference in the first time step and the eddy diffusion terms.

The domain is divided into 500 m grid squares. A 7.5 sec time increment has been adopted as a time interval short enough to satisfy the requirement for computational stability. Numerical time integrations are carried out during half an hour in order to cover the life-cycle of convection in several cases (Table 1).

Table 1. Initial conditions for basic field.

Case	Surface temperature $T_0(0)$ (°C)	Lapse rate γ_0 (°C/1 km)	Relative humidity (%)	Vertical shear (m sec ⁻¹ /1 km)
1	15	10	0	5
2	15	10	0	0
3	15	6.5	100	5
4	15	6.5	100	0
5	30	6.5	100	5
6	30	6.5	100	0

It can be seen that the data reduce to two principal types of case: a dry layer with slight absolute instability and a moist layer with conditionally unstable stratification, respectively. The former case is adopted to avoid complexity caused by the release of latent heat and not to lose essential dynamical effect of vertical shear. Each case is compared with corresponding ones without vertical shear, respectively.

Initial fields of motion, temperature and moisture are composed of their horizontally uniform basic fields listed in Table 1 and the deviations from their basic ones. No disturbed motion is assumed initially. The temperature disturbance T' which produces buoyancy triggering convective motion is given in a sinusoidal form only in the lower half layer (Fig. 1).

$$T' = -T_a(z) \cos \frac{2\pi}{L}x \quad (5.1)$$

$$T_a > 0 \quad \text{when } z < 2 \text{ km}$$

$$T_a = 0 \quad \text{when } z \geq 2 \text{ km}$$

where $L=10$ km and the maximum tempera-

ture deviation is 1.25°C at the level of 1 km. The moist layers saturated with water vapor are assumed throughout except for cases 1 and 2. Thus the specific humidity is determined by using the temperature described above and the associated standard atmospheric pressure.

6. Results

A convective motion which is generated by buoyancy applied initially is followed successively through a life cycle. Here we will primarily pay attention to cases 1 and 3.

1) Evolution of convection

Both motion and temperature fields in case 1 are shown at 8, 12 and 16 min of the elapsed time in Figs. 2 and 3. Each figure is arranged to include representatives of the various stages of the life-cycle such as developing, mature and decaying stages.

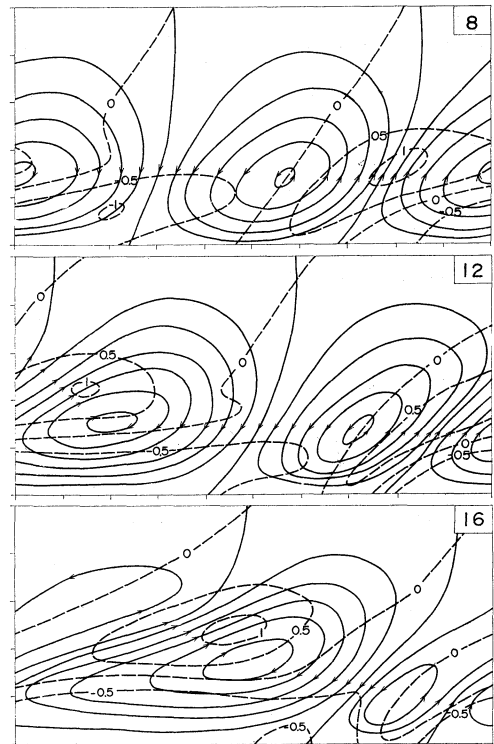


Fig. 2. Motion and temperature fields deviated from their initial basic ones in case 1. Solid lines with arrows are streamlines at every $10^3 \text{ m}^2 \text{ sec}^{-1}$ and temperature excess from initial basic field is shown in broken lines at every 0.5°C . Elapsed time is illustrated at each upper right corner in min.

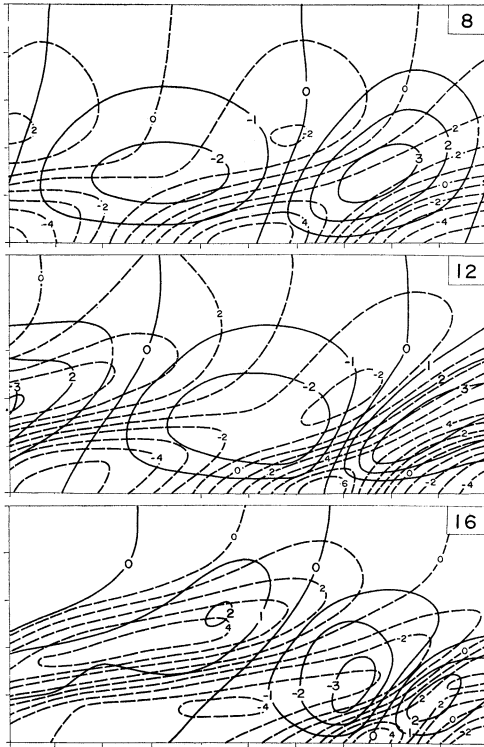


Fig. 3. Vertical (solid lines) and horizontal (broken lines) components of velocity corresponding to the motion in Fig. 2. They are drawn at every 1 m sec^{-1} .

Fig. 2 shows the streamlines of the motion deviated from its initial basic one (solid lines with arrows) and the temperature deviation from its initial basic one (broken lines). In Fig. 3, the vertical and the horizontal components of the motion deviated from its initial basic one are drawn in solid and broken lines, respectively. The convective motion grows with time for 12 min. In this stage, the narrowing updraft region and the widening downdraft region are observed to a lesser degree than would be expected in a conditionally unstable layer. This phenomena, which is not usually expected in an absolutely unstable layer, may depend on the initial temperature disturbance imposed in the lower layer. Then, the maximum upward velocity attains 3.9 m sec^{-1} at the 1.5 km level and the maximum temperature excess becomes 1°C . Both of them are larger than the maximum downward velocity, 2.9 m sec^{-1} , and the maximum temperature deficit, 0.8°C .

The position of the warm core is well coincident with that of the convection core; the latter being defined as the maximum upward velocity. After 12 min the convective motion begins to decrease and is accompanied by the stabilization of the lower layer.

In order to illustrate the effect of vertical shear Figs. 4 and 5 are presented. These show the evolution of convection under the same condition as case 1 except that no basic

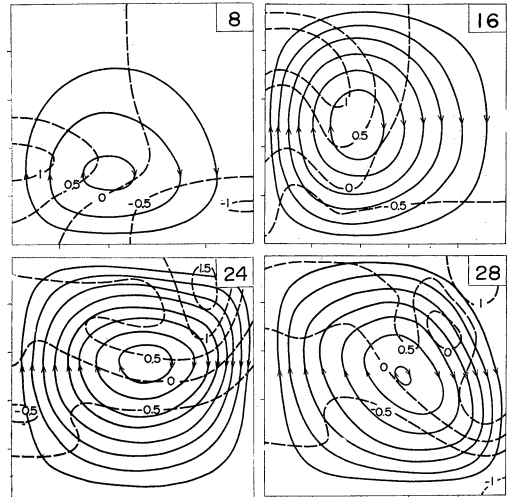


Fig. 4. Motion and temperature fields in case 2 as in Fig. 2. Streamlines are drawn at every $2 \times 10^3 \text{ m}^2 \text{ sec}^{-1}$ and temperature excess at 0.5°C .

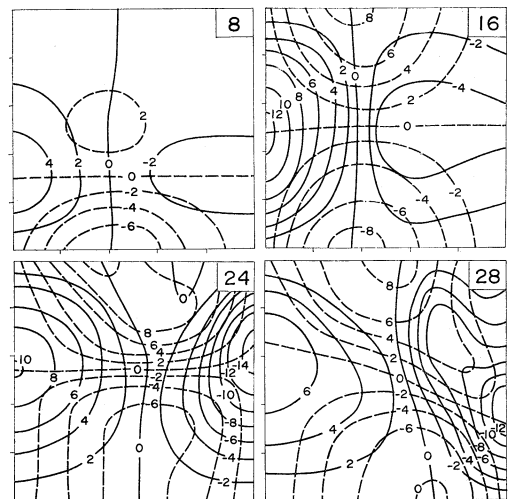


Fig. 5. Vertical and horizontal components of velocity at every 2 m sec^{-1} in case 2 as in Fig. 3.

flow is considered. Since the convection will be symmetrical about the $y-z$ coordinate plane, only the right half of the domain is listed here. In this case (without vertical shear), the convective motion is intensified much more than that in case 1 (with vertical shear) and continues to grow for 22 min. As a result, the maximum upward velocity attains 12 m sec^{-1} at the 2.5 km level after 18 min. During this period, the warm air in the lower layer is replaced by the cold air in the upper layer through the process of warm air ascending and the cold air descending. The overturning is completed 22 min after the convective motion started and then the circulation decreases with time and changes into the damping stable oscillation characterized by the alternate opposite direction.

Figs. 6 and 7 show the motion and the temperature fields deviated from their initial basic ones at every 4th minutes in case 3 as

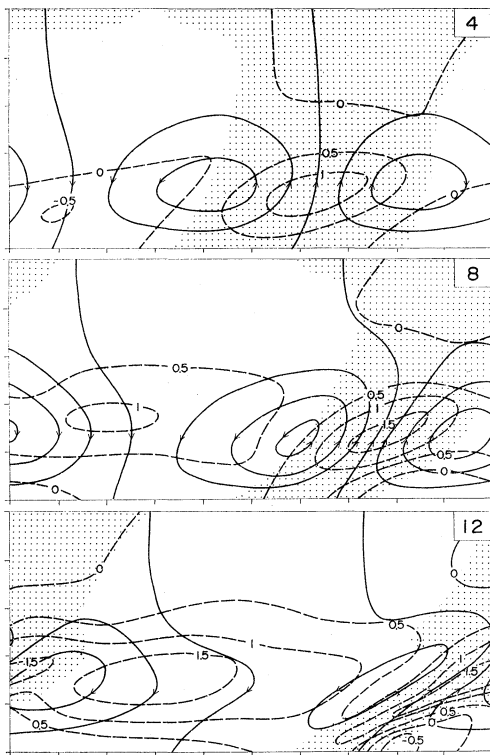


Fig. 6. Motion and temperature fields in case 3 as in Fig. 2. Streamlines are drawn at every $10^3 \text{ m}^2 \text{ sec}^{-1}$ and temperature excess at 0.5°C . Regions saturated with water vapor are stippled.

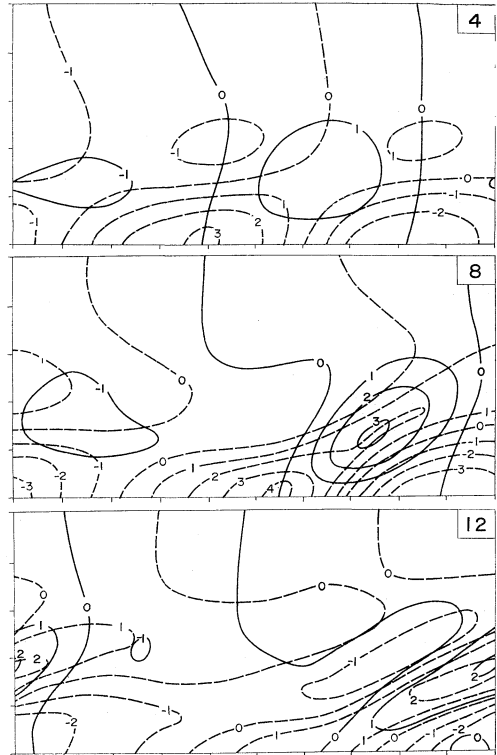


Fig. 7. Vertical and horizontal components of velocity at every 1 m sec^{-1} in case 3 as in Fig. 3.

in case 1. The regions saturated with water vapor are indicated by stippling in Fig. 6. The association of the intensification of convection with the narrowing updraft region and the widening downdraft region is remarkable. These regions are favorable for attaining the surplus heating in the ascending motion, necessary for promoting the subsequent development. The convective motion grows for 8 min at the end of which the maximum upward velocity attains 3.2 m sec^{-1} (three times larger than the maximum downward velocity) and the maximum temperature excess reaches 1.6°C around the convection core. In this moist convection, the downdraft region, as well as the updraft region, is heated. This, of course, is different from a dry convection in an absolutely unstable layer such as case 1. Finally, the convection plunges into the decaying stage without extending the convective circulation to the upper layer.

In case 4 (the result of which is not

illustrated here), the development of convective motion is more intensive than that in case 3 and continues until the 22nd min. In either case there is no doubt that the development of convection is suppressed in the basic flow with vertical shear.

2) *Displacement and configuration of convection cell*

One of the most important differences between the characteristics of convections in the cases with and without vertical shear is concerned with the configurations of the convections. The symmetry of the convection cell is destroyed in the case with vertical

shear as illustrated in Figs. 2-7. As an example the displacement of the convection cell in case 1 is shown by indicating the positions of the significant axes at every 4 min interval in Fig. 8. The central axes of upward motion and of warm region are illustrated in this figure by solid and broken lines, respectively.

We can find that the convection axis tilts downwind with height and its slope increases with time during the developing stage. However, the tilt is quite small compared with that which would be expected due only to horizontal advection indicated in slight broken lines. The convection core rises and soon the lower layer is occupied by the stable oscillation regime. Therefore the convection axis may be insignificant especially in the lower layer. It should be noted that the rising convection core moves nearly at the speed of basic flow at its level.

Furthermore, the central axis of warm region tilts downwind with height so steeply that it is further ahead of the axis of updraft at higher levels than the convection core and behind it in the lower levels. The phase difference between them makes upward heat transport smaller than in case 2. On the other hand, the tilt of the convection axis gives rise to the vertical transport of horizontal momentum. These are concerned with energy transformation of convection described below.

3) *Vertical transport of heat*

The vertical transport of sensible heat is

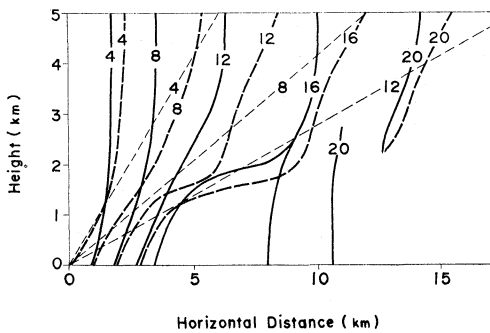


Fig. 8. Horizontal displacement with time of the convection cell in case 1. The ordinate is the height and the abscissa is the horizontal distance from the initial central axis in km. The central axes of upward motion and of warm region are illustrated in solid and broken lines at every 4 min, respectively.

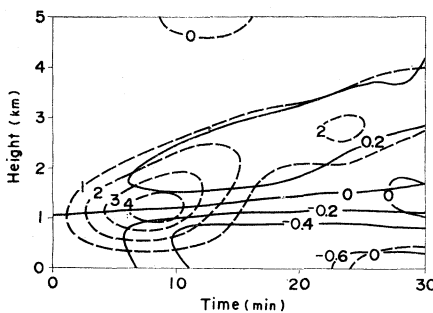


Fig. 9(a). Variation with time of the vertical distribution of horizontally averaged temperature excess ($^{\circ}\text{C}$) and vertical transport of sensible heat (arbitrary unit) indicated by solid and broken lines, respectively in case 1.

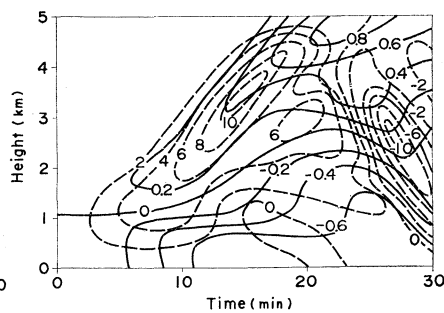


Fig. 9(b). Case 2. Same as in Fig. 9(a).

associated with the energy transformation of potential energy into kinetic energy which is able to excite convective motion. Figs. 9(a) and (b) show the variation with time of the vertical distribution of horizontally averaged temperature excess and the vertical transport of sensible heat in cases 1 and 2, respectively.

In case 2, the upward heat transport is observed until approximately the 24th min during the developing stage without vertical shear. As a result, the temperature excess and deficit becomes about 0.8°C at the highest and the lowest levels, respectively. This makes the initial (slightly unstable) stratification tend to neutralize, that is, approach the dry adiabatic lapse rate of $9.77^{\circ}\text{C}/\text{km}$. Afterwards, the decay of convection begins to be associated with the downward heat transport and soon will bring about the stable oscillation.

Fig. 9(a), in case 1 with vertical shear, shows that the upward heat transport is less than that in the former case, although it continues through 30 min. In general, until 12 min has passed, the rather large upward heat transport diminishes the instability in the lower 2 km layer and the stabilization of the upper layer proceeds extremely slowly due to inactive convective motion.

Figs. 10(a) and (b) illustrate cases 3 and 4, respectively similarly to Fig. 9(a). In these cases, the horizontally averaged temperature is affected by the release of latent heat $\overline{S_0 w}$ as well as the divergence of the vertical sensible heat flux. Warming of the layer continues until the 24th min in the whole domain in case 4, while it ceases after the 12th min in case 3 and is almost confined to the lower half layer.

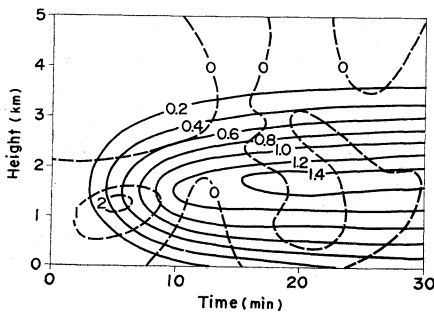


Fig. 10(a). Case 3. Same as in Fig. 9(a).

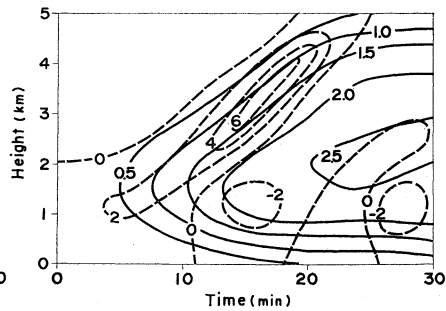


Fig. 10(b). Case 4. Same as in Fig. 9(a).

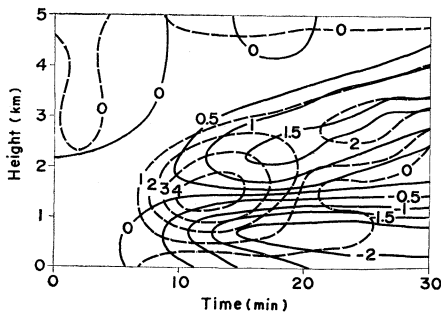


Fig. 11. Variation with time of the vertical distribution of horizontal average of horizontal velocity deviated from its initial (m sec^{-1}) and vertical transport of horizontal momentum ($\text{m}^2 \text{sec}^{-2}$) indicated by solid and broken lines, respectively in case 1.

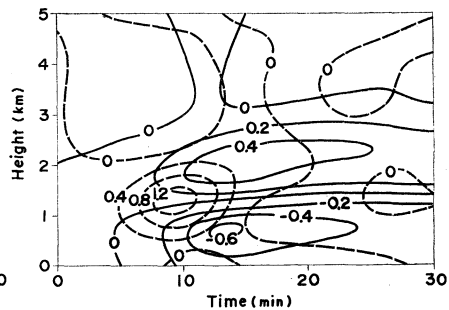


Fig. 12. Case 3. Same as in Fig. 11.

4) Vertical transport of momentum

Another important energy transformation is made due to the vertical transport of horizontal momentum \overline{uw} in the layer with vertical shear. This results in the interaction between convection and basic flow.

Figs. 11 and 12 illustrate for cases 1 and 3, respectively, (1) the variation with time of the vertical distribution of the horizontal average of horizontal velocity deviated from its initial and, (2) the vertical transport of horizontal momentum. The features of the vertical transport of horizontal momentum are similar to those of sensible heat, whereas the maximum values of the upward momentum transport occur several minutes later than those of sensible heat. This suggests that the convection first grows through the transformation of potential into kinetic energy. The reason for this is because of the upward heat transport. When the convection has developed fairly well the upward momentum transport increases with time and becomes effective to suppress more development of convection and make it decay rapidly.

7. Energy transformation

The variation with time of various kinds

of energies defined in Section 4 in cases 1 and 2 are shown in Figs. 13(a) and (b), respectively. The mean potential energy does not change through the dry convection such as in cases 1 and 2 because of no heat source and sink. In order to simplify our energy consideration, the variation with time of energy transformations and of the rates of change in time of energies are shown in Figs. 14(a) and (b) for cases 1 and 2, respectively.

In case 2 without vertical shear the kinetic energy of convection (measured by $\langle K_e \rangle$) increases until the 24th min. It is associated with the decrease of potential energy. This case provides quite a simple energy transformation in a life cycle of convection. Namely, upward heat transport gives rise to the transformation of potential into kinetic energy. This results in the development of convection until the 24th min. Some disagreement between the time rates of potential and kinetic energies can be attributed to the dissipative effect of eddy viscosity. As shown in Fig. 9(b), the unstably stratified layer is completely dissolved after 24th min. It then oscillates around neutral stratification and begins to be associated with the alterna-

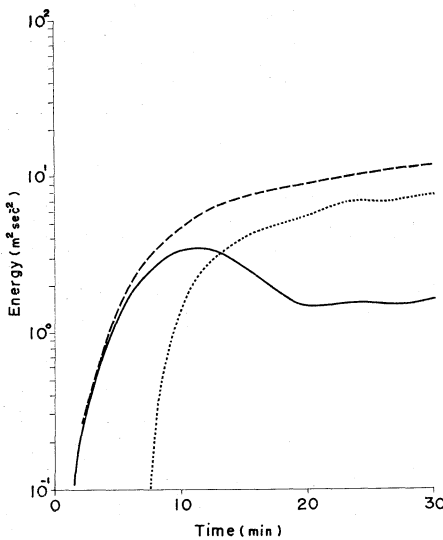


Fig. 13(a). Variation of energy with time in case 1. $\langle K_e \rangle$ is indicated by solid line, $-\langle P_e \rangle$ by broken line and $\langle K_m \rangle$ by dotted line.

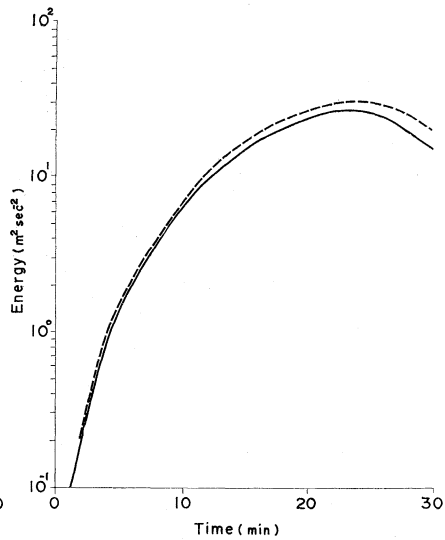


Fig. 13(b). Case 2. Same as in Fig. 13(a).

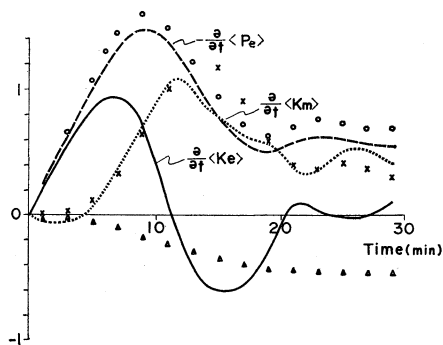


Fig. 14(a). Variation with time of energy transformations and of the rates of change of energies in case 1 (arbitrary unit). Circles denote $\langle gT^*w \rangle$, crosses $\langle uw(\partial\bar{u}/\partial z) \rangle$ and triangles $-\langle D_k \rangle$.

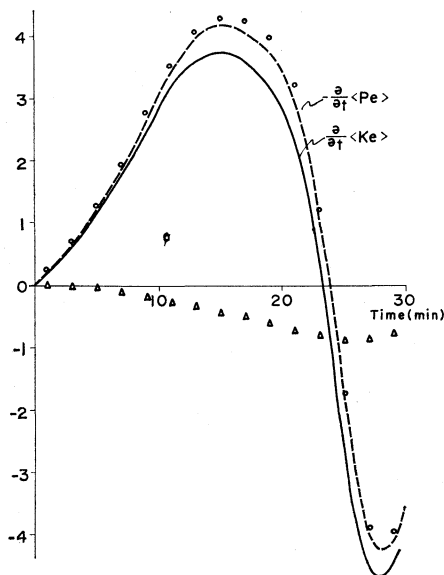


Fig. 14(b). Case 2. Same as in Fig. 14(a).

tion of direction of heat transport and, hence, energy transformation.

In case 1, with vertical shear, (Figs. 13(a) and 14(a)), we have another type of energy transformation. The transformation is due to vertical transport of momentum taking part in the above process. There is hardly difference between both cases in the early stage. However, the axis of updraft does not coincide with that of temperature. Consequently, the heat transport becomes small compared with that in case 2. In addition to this, the tilt of axis downwind with height causes upward transport of horizontal momentum. This results in the transformation of eddy into mean kinetic energy. Soon, the latter transformation tends to overcome the former transformation. Thus, the convection develops less than that in case 1 and changes into the decaying stage after 12 min. The upward transport of sensible heat and horizontal momentum persists only slowly after the decaying stage is entered.

Fig. 15(a) and (b) show the variation of energy with time in cases 3 and 4. These

cases introduce the decrease of mean potential energy due to the release of latent heat in a conditionally unstable layer. Fig. 16(a) and (b) illustrate the variation with time of energy transformations and of the rates of change of energies in cases 3 and 4.

In the first place, the convective motion generated by the initial buoyancy causes the release of latent heat due to condensation in the updraft region. Although the convection grows at the expense of eddy potential energy, heating due to the release of latent heat predominates in the lower layer so as to increase eddy potential energy as a whole. Thus, in the early stage we can find that eddy potential energy, as well as eddy kinetic energy, increases with time. As described in case 1, the upward transport of horizontal momentum becomes effective to suppress more development of the convection in case 3. Therefore the development of the convection is so weak that it enters into the decaying stage earlier than in case 4 without vertical shear. So we can conclude that a basic flow with vertical shear has the suppressive

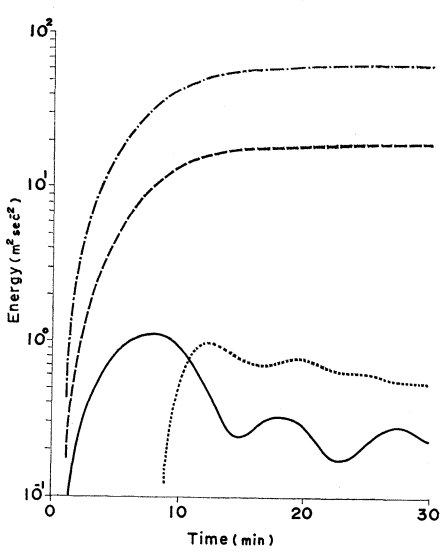


Fig. 15(a). Variation of energy with time in case 3. $\langle K_e \rangle$, $\langle K_m \rangle$, $\langle P_e \rangle$ and $-\langle P_m \rangle$ are indicated by solid, dotted, broken and chain lines, respectively.

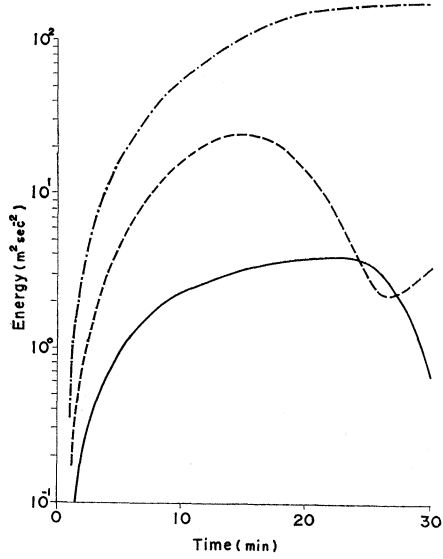


Fig. 15(b). Case 4. Same as in Fig. 15(a).

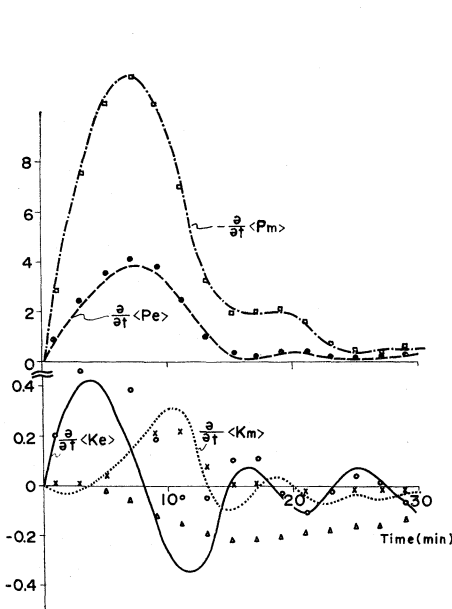


Fig. 16(a). Variation with time of energy transformations and of the rates of change of energies in case 3. Dots denote $\langle \phi'' S_0 w \rangle$, squares $-\langle \phi \rangle$, $\langle S_0 w \rangle$ and the others are the same as in Fig. 14(a).

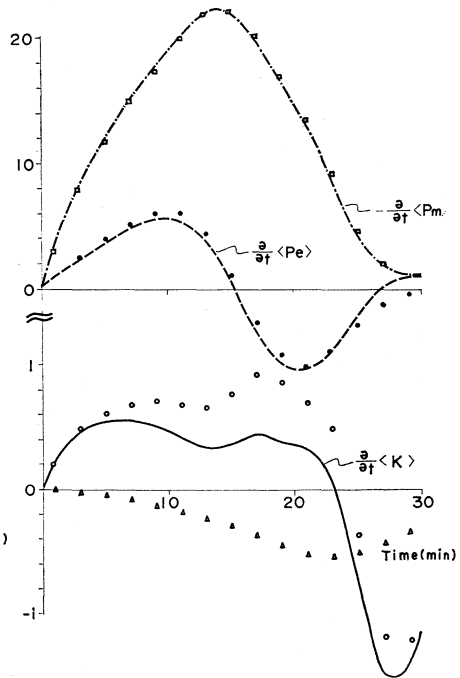


Fig. 16(b). Case 4. Same as in Fig. 16(a).

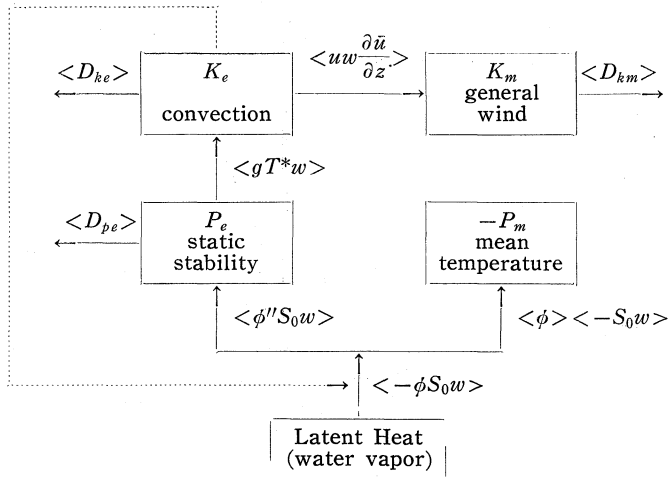


Fig. 17. Energy flow diagram for cumulus convection.

effect on the convection in the plane parallel to its direction. This is due to both the transformation of eddy kinetic energy into mean kinetic one and the weakness of the transformation of potential energy into kinetic one.

Finally, the energy flow diagram is illustrated in Fig. 17 to summarize the above discussion. Fig. 17 indicates the path of the energy flow if the associated transformation $\langle \rangle$ is positive. Numerical experiments in the present model also show the energy flow to the direction of the arrows indicated in Fig. 17 through almost an entire life-cycle of convection.

Acknowledgement

The author wishes to express his hearty thanks to Dr. H. Arakawa, Dr. K. Takahashi, Prof. S. Hayami and Assistant Prof. R. Yamamoto of Kyoto University for their encouragement throughout this study. The author is indebted to Dr. S. Matsumoto and the members of his laboratory for stimulating discussions exchanged with him.

References

- Asai, T., 1960: Numerical experiment of convection in the model atmosphere. Proc. International Symposium on Numerical Weather Prediction in Tokyo, Meteor. Soc. Japan, pp. 469-476.
- , 1964: Numerical experiment of cumulus convection under the pseudo-adiabatic process. To be published.
- Atlas, D., *et al.*, 1963: Severe local storms. Meteorological Monographs, 5, 27, 247 pp.
- Browning K. A. and F. H. Ludlam, 1962: Airflow in convective storms. Quart. J. roy. meteor. Soc., 88, 117-135.
- Brunt, D., 1951: Experimental cloud formation. Compendium of Meteorology. pp. 1255-1262.
- Byers, H. R. and R. R. Braham, 1949: The Thunderstorm. U. S. Department of Commerce, 287 pp.
- Byers, H. R. and L. J. Battan, 1949: Some effects of vertical wind shear on thunderstorm structure. Bull. Amer. Meteor. Soc., 30, 168-175.
- Chao, Jih-ping, 1961: On the dynamics of development of thermal convection in a stratified atmosphere. Acta Meteorologica Sinica, 31, 191-204.
- Conover, J. H., 1960: Cirrus patterns and related air motions near the jet stream as derived by photography. J. Meteor., 17, 532-546.
- Hitschfeld, W., 1960: The motion and erosion of convective storms in severe vertical wind shear. J. Meteor., 17, 270-282.
- Jeffreys, H., 1923: Some cases of instability in fluid motion. Proc. Roy. Soc., (A) 118, 195-208.
- Kuo, H. L., 1963: Perturbations of plane couette flow in stratified fluid and origin of cloud streets. The Physics of Fluids, 6, 195-211.
- Kuettner, J., 1959: The band structure of the atmosphere. Tellus, 11, 267-294.
- Ligda, M. G. H., 1956: Study of the synoptic application of weather radar data. Final Rep., Contract AF 19 (604)-573, A. and M. College of Texas.
- Lilly, D. K., 1962: On the numerical simulation of buoyant convection. Tellus, 14, 148-172.

- Malkus, J. S., 1952: The slopes of cumulus clouds in relation to external wind shear. *Quart. J. roy. Meteor. Soc.*, **78**, 530-542.
- Malkus, J. S. and G. Witt, 1959: The evolution of a convective element; a numerical calculation. *The atmosphere and the sea in motion*, New York, Rockefeller Institute Press, pp. 425-439.
- Newton, C. W. and H. R. Newton, 1959: Dynamic interactions between large convective clouds and environment with vertical shear. *J. Meteor.*, **16**, 483-496.
- Ogura, Y., 1962: Convection of isolated masses of buoyant fluid: a numerical calculation. *J. Atmos. Sci.*, **19**, 492-502.
- , 1963: The evolution of a moist convective element in a shallow, conditionally unstable atmosphere: a numerical calculation. *J. Atmos. Sci.*, **20**, 407-424.
- Ogura, Y. and N. A. Phillips, 1962: Scale analysis of deep and shallow convection in the atmosphere. *J. Atmos. Sci.*, **19**, 173-179.
- Phillips, N. A., 1956: The general circulation of the atmosphere: a numerical experiment. *Quart. J. roy. Meteor. Soc.*, **82**, 123-164.
- Spiegel, E. A. and G. Veronis, 1960: On the Boussinesq approximation for a compressible fluid. *Astrophysical Jour.*, **131**, 442-447.

風の鉛直シャーがある大気中での積雲対流

— 数 値 実 験 —

浅 井 富 雄

(気 象 研 究 所)

力学方程式系の数値時間積分に基づき、鉛直シャーのある風系中における積雲対流の性状が調べられる。ここでは、運動は鉛直面内で、非発散、偽断熱の条件のもとで取扱われる。ただし運動量、熱及び水蒸気のうず交換は考慮に入れられる。

鉛直シャーのある場合とない場合について、それぞれ対流の時間的发展過程及びエネルギー変換が示される。それによれば、鉛直シャーのある場合には、対流の軸対称性は崩れ、対流軸は高さとともに風下の方へ傾く。その結果、対流から基本流へ向かう運動エネルギーの変換が生じ、対流の発展が抑制される傾向にある。更に上昇流の中心軸と温暖域の中心軸との不一致が生じ、これは位置エネルギーから対流運動エネルギーへの変換量を減じさせる。